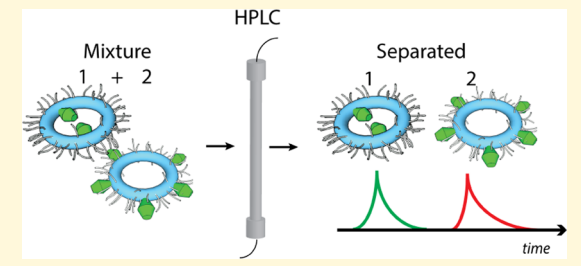


## Inner and Outer Surface Functionalizations of Ultrasmall Fluorescent Silica Nanorings As Shown by High-Performance Liquid Chromatography

Melik Z. Turker, †,#© Thomas C. Gardinier,†,#© Joshua A. Hinckley,‡© Cintia B. Contreras, Fem Woodruff, $^{\$}$  Kai Ma,†, $^{\dagger,\perp}$ © Ferdinand F. E. Kohle,‡© and Ulrich B. Wiesner\*,†©

## Supporting Information

ABSTRACT: In the past two decades, ultrasmall fluorescent nanomaterials have garnered significant interest in the fields of bioimaging and nanomedicine. More recently, attention has shifted from purely spherical nanoparticles to objects with a variety of different shapes, such as high-aspect-ratio, hollow, and star-shaped nanomaterials. We have recently reported the synthesis and characterization of ultrasmall silica nanoparticles with complex shapes, including silica nanocages, silica nanorings, and single-pore silica nanoparticles. Here, we focus on fluorescent silica nanorings that are of particular interest for theranostic applications in nanomedicine. We present in-depth studies of the



synthesis and orthogonal surface functionalization, successfully distinguishing the inside and outside of the silica nanorings, utilizing a combination of spectroscopic and analytical techniques including fluorescence correlation spectroscopy and reversedphase high-performance liquid chromatography. Results suggest that despite the small silica ring diameter of around 10 nm and below, it is possible to effectively "hide" hydrophobic moieties on the inside of the rings but that their number must be carefully engineered. We expect the chemistry and methods developed here to be of interest to a range of differently shaped porous nanoparticles within the ultrasmall-size regime.

## INTRODUCTION

In the past two decades, the field of ultrasmall nanoparticles (NPs) with sizes below 10 nm and potential applications ranging from catalysis to nanomedicine have garnered significant interest. 1-3 While early efforts focused on dense spherical NPs, the field has since expanded to NPs with a variety of forms and shapes including high-aspect-ratio materials (i.e., rods and worms), star-shaped NPs, as well as nanocages. 4-6 These classes of NPs are distinguished from their spherical counterparts by often having multiple types of distinct surfaces, which can potentially be functionalized with different chemistries.7-9 Mesoporous silica-based NPs have played a crucial role in this context as the typical surfactantbased template synthesis approach enables straightforward functionalization of inside and outside surfaces with orthogonal chemistries. 10,11 The resulting silica nanomaterials have many advantages, including robust synthetic protocols and highpotential drug payloads. 10,12 They do not, however, typically activate the renal pathway for rapid whole-particle excretion in mammalian organisms, which requires particle diameters below the cutoff for renal clearance, i.e., below ~10 nm, thereby lowering the potential for adverse side effects. 13,14 To overcome this challenge, in addition to spherical silica

nanoparticles (SNPs), our group has recently reported the synthesis and characterization of ultrasmall SNPs with a number of different morphologies including single-pore mesoporous SNPs, silica nanorings, and silica nanocages. 3,9,15,16 These types of NPs are of particular interest as they provide a pathway for clinical translation as a result of proven favorable biodistribution and pharmacokinetics profiles of ultrasmall SNPs, 3,17,18 while simultaneously offering distinguishable "inside" and "outside" surfaces for orthogonal functionalization critical for surface-directed multifunctionalization of NPs. 10,19 Spherical multifunctional fluorescent oxide NPs have previously been reported with only one (outside) surface type available for ligand conjugation, 20,21 but having two distinct surfaces in combination with ultrasmall particle sizes offers unique advantages, e.g., in therapeutic applications in nanomedicine, as well as other applications such as the selfassembly of NPs. 9,22,23

To take advantage of distinct surfaces such as those present in ultrasmall torus-shaped mesoporous NPs or nanorings, the

Received: March 28, 2019 Revised: June 28, 2019 Published: July 16, 2019



<sup>&</sup>lt;sup>†</sup>Department of Materials Science and Engineering, <sup>‡</sup>Department of Chemistry and Chemical Biology, and <sup>§</sup>Robert Frederick Smith School of Chemical and Biomolecular Engineering, Cornell University, 330 Bard Hall, Ithaca, New York 14853, United States

Nanosystems Institute, National University of San Martin, San Martin B1650, Buenos Aires, Argentina

<sup>&</sup>lt;sup>1</sup>Elucida Oncology Inc., New York, New York 10016, United States

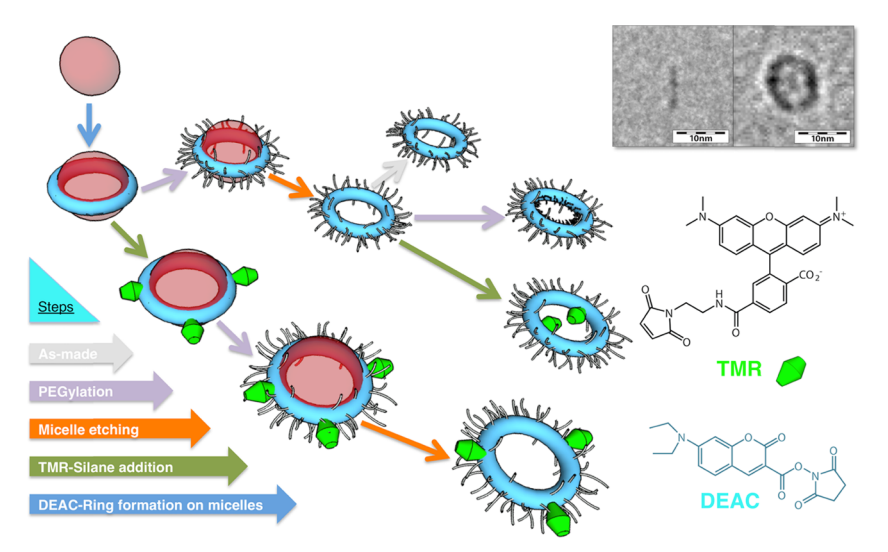


Figure 1. Steps (bottom left, not in a representative sequence) to orthogonally PEGylate and functionalize inside and outside surfaces of ultrasmall silica nanorings. Surfactant micelles represented in red (top left) act as templates for silica nanoring growth (blue arrow), simultaneously encapsulating 7-diethylaminocoumarin-3-carboxylic acid (DEAC) dye in the silica matrix. After dyed silica nanoring formation, individual steps along two different pathways are taken to be able to specifically PEGylate and/or functionalize the outside (bottom sequence) and inside (top sequence) surfaces of the rings. Individual steps include PEGylation (purple arrows), micelle removal (orange arrows), and tetramethylrhodamine (TMR)-silane additions (green arrows). Representative cryo- and transmission electron microscopy (cryo-EM/TEM) images show two orthogonal projections of a silica nanoring (edge-on, left; planar, right) formed around a trimethyl benzene (TMB)-swollen hexadecyltrimethyl ammonium bromide (CTAB) micelle (top right).

surface chemistry must be carefully characterized. Surface chemistry assessments of NPs remain challenging, however, as results of standard characterization techniques such as  $\zeta$ potential measurements or dynamic light scattering are often limited to ensemble measurements, which do not offer a comprehensive description of the heterogeneity of surface chemical NP properties within a single sample batch.<sup>24-26</sup> In contrast to larger-sized mesoporous SNPs where inside and outside surfaces are well defined, these difficulties are exacerbated for ultrasmall NPs like silica nanorings, as the distinction between inside and outside may not be straightforward as a result of the geometry of the object (see Figure 1). We recently reported a method to analyze the surface chemistry of spherical ultrasmall fluorescent SNPs using high-performance liquid chromatography (HPLC).2 HPLC is a ubiquitous and well-established technique for the characterization of small molecules, synthetic macromolecules, and proteins, <sup>28-30</sup> but before our study had not been applied for the characterization of solid inorganic core-organic ligandbased core-shell NPs. Since ultrasmall NPs have sizes comparable to medium-sized macromolecules/proteins, we demonstrated that HPLC in combination with gel permeation chromatography (GPC) is indeed a very powerful tool to quantitatively assess heterogeneities in surface chemical properties of spherical particles (via HPLC) and their correlations to size (via GPC).<sup>27</sup> In the present study, we apply a combination of GPC and HPLC to the characterization of fluorescent silica nanorings, mesoporous torus-shaped nanomaterials with a single pore, as a testbed for attempting to differentiate between inside and outside surfaces of the rings. For convenience, we will refer to these nanomaterials as Cornell rings or simply C rings. We successfully demonstrate that HPLC is a rapid and reliable screening tool capable of differentiating the locations of ligands conjugated to either of the two surfaces of these torus-shaped objects. Furthermore, we observe a transition regime in which, as a function of

synthesis conditions, the ring's inner pore becomes too crowded resulting in the ligands being pushed more and more out of the inner pore of the rings. For a given dye-ligand model, using HPLC in combination with other characterization techniques including fluorescence correlation spectroscopy (FCS), we are able to define an upper limit of effective ligand loading to the inner surface of the nanorings. We expect that our synthesis and characterization method development, enabling first the orthogonal preparation of such ligandfunctionalized silica nanorings and subsequently the quantitative characterization of the distribution of ligands between inside and outside surfaces of such ultrasmall torus-shaped SNPs, will be of interest to other NP systems. Furthermore, the specific silica nanorings described herein constitute interesting vehicles for theranostic, i.e., combined therapeutic and diagnostic, applications in nanomedicine in general and oncology in particular.

# MATERIALS AND METHODS/EXPERIMENTAL SECTION

Materials. All materials were used as received. 7-Diethylaminocoumarin-3-carboxylic acid, succinimidyl ester (DEAC), and tetramethylrhodamine-6 C2 maleimide (TMR) were purchased from Anaspec. Cyanine5 maleimide (Cy5) with a net positive charge was purchased from Lumiprobe. Sulfo-cyanine5 maleimide (sulfo-Cy5) with a net negative charge was purchased from Click Chemistry Tools. Hexadecyltrimethyl ammonium bromide (CTAB, ≥99%), tetramethyl orthosilicate (TMOS, ≥99%), 2.0 M ammonium hydroxide in ethanol, and anhydrous dimethyl sulfoxide (DMSO, ≥99%) were purchased from Sigma-Aldrich. (3-Aminopropyl)trimethoxysilane (APTES), 2-[methoxy (polyethyleneoxy) 6-9propyl]trimethoxysilane (PEG-silane, 6-9 ethylene glycol units), (3-mercaptopropyl)trimethoxysilane (MPTMS, 95%), and methoxy triethyleneoxy propyl trimethoxysilane (PEG-silane, three ethylene glycol units) were obtained from Gelest. Mesitylene (TMB, 99% extra pure) was purchased from Acros Organics. Absolute anhydrous ethanol (200 proof) was purchased from Koptec. Glacial acetic acid was purchased from Macron Fine Chemicals. Sodium chloride

irrigation USP solution (5.0 M) was purchased from Santa Cruz Biotechnology. Syringe filters (0.2  $\mu$ m, poly(tetrafluoroethylene) (PTFE) membrane) were purchased from VWR International. Vivaspin sample concentrators (molecular weight cut-off (MWCO) 30k) and Superdex 200 prep grade were obtained from GE Health Care. Snakeskin dialysis membrane (MWCO 10k) was purchased from Life Technologies. Deionized water was generated using a Millipore Milli-Q system (18.2 M $\Omega$  cm). Glass-bottom microwell dishes for FCS were obtained from MatTek Corporation. Carbonfilm-coated copper grids for TEM were purchased from Electron Microscopy Sciences. UHPLC-grade acetonitrile was purchased from BDH. Xbridge protein BEH C4 column (300 Å, 3.5  $\mu$ m, 4.6 mm  $\times$ 150 mm, 10k-500k) and BioSuite high-resolution size exclusion column (250 Å, 5  $\mu$ m, 7.8 mm × 300 mm, 10k-500k) were purchased from Waters Technologies Corporation. Trifluoroacetic acid was purchased from Neta Scientific.

Conjugation of Fluorescent Dyes DEAC, TMR, and Cy5. For a 10 mL batch reaction, a 0.2  $\mu$ mol succinimidyl ester derivative of DEAC dye was conjugated with 5  $\mu$ mol APTES (1:25 ratio) in 100  $\mu$ L DMSO for the synthesis of C rings that have DEAC dye covalently encapsulated in the silica matrix. For inner or outer surface dye functionalization of a 10 mL reaction batch, 0.4  $\mu$ mol of a maleimido derivative of TMR dye was conjugated with 10  $\mu$ mol of MPTMS (1:25 ratio), and 0.18  $\mu$ mol of Cy5 was conjugated with 4.2  $\mu$ mol MPTMS (1:23 ratio) in 100  $\mu$ L DMSO. All of the dye conjugations were made 1 day prior to their use in the synthesis by mixing the components by pipette and leaving the solution overnight in the glovebox.

Synthesis of PEGylated Fluorescent C Rings. Fluorescent C rings were synthesized in aqueous solution using surfactant micelles templating the silica condensation. For a 10 mL batch reaction, 83 mg of CTAB was dissolved in 9 mL of deionized water, and 1 mL of ammonium hydroxide solution (0.02 M) was added to the reaction in a 25 mL round-bottom flask. The solution was stirred at 600 rpm at 30 °C for 30 min before the addition of 100  $\mu L$  TMB to expand the micelles, which was followed by stirring for 1 h. Afterward, 68  $\mu$ L TMOS and a 100  $\mu$ L DEAC dye conjugate were added into the solution in subsequent steps, and the reaction was left stirring overnight at 30 °C. The following day, 100 µL PEG-silane (6-9 ethylene glycol units) was added into the 10 mL reaction under stirring at 600 rpm, and the solution was left stirring overnight at 30 °C. The concentrations of TMOS, CTAB, TMB, and PEG-silane were approximately 45.6, 22.7, 71.9, and 21.5 mM, respectively. The next day after PEG-silane addition, the sample solution was heated at 80 °C overnight without stirring to enhance covalent PEG-silane condensation.3

**Purification of C Rings.** The day after 80 °C heating, the solution was cooled down to room temperature, syringe-filtered (MWCO 0.2  $\mu$ m, PTFE), and transferred into a dialysis membrane (MWCO 10k). Then, the sample was dialyzed in 200 mL of ethanol/deionized water/glacial acetic acid solution (500:500:7 volume ratio), and the acid solution was changed once a day for 3 days to remove/etch CTAB from the pores of the C rings (micelle removal) and to remove unreacted reagents from the sample. Following the acid dialysis, the sample was transferred into 5 L deionized water, and the water was refreshed once a day for 3 days to remove ethanol and acetic acid solvents.

Synthesis of Inner-Surface-PEGylated Fluorescent C Rings. Following all of the purification and CTAB micelle removal steps to have the C ring pores accessible for inner surface functionalization, 400  $\mu$ L of PEG-silane (three ethylene glycol units) was added into 10 mL of the C ring native synthesis solution (estimated concentration 6  $\mu$ M) in a 25 mL round-bottom flask under stirring at 600 rpm at room temperature. The solution was left stirring overnight. The concentration of PEG-silane (three ethylene glycol units) was roughly 142 mM.

Synthesis of Inner Surface Dye-Functionalized Fluorescent C Rings. Following all of the purification steps and CTAB micelle removal steps to have the C ring pores accessible for inner surface functionalization, 100  $\mu$ L of TMR-silane conjugate in DMSO was

added into 10 mL of native C ring synthesis solution in a 25 mL round-bottom flask under stirring at 600 rpm and room temperature overnight. The concentration of TMR dye was roughly 40  $\mu$ M. For the dye-loading series experiments, TMR concentrations were varied between 10 and 120  $\mu$ M (see the main text).

Synthesis of Outer Surface Dye-Functionalized Fluorescent C Rings. Following the same procedure for the first day of the fluorescent C ring synthesis described above, 100  $\mu$ L of the TMR-silane conjugate DMSO solution described in the previous section was added into 10 mL of native C ring synthesis solution (with C rings still containing the CTAB micelles), just before the addition of PEG-silane (6–9 ethylene glycol units) to the outer surface of the rings in a 25 mL round-bottom flask under stirring at 600 rpm at room temperature.

Synthesis of Inner/Outer Surface Dye-Functionalized Blank C Rings. For the synthesis of inner/outer surface dye-functionalized blank C rings, the addition of conjugated DEAC dye was skipped after the addition of TMOS on the first day of synthesis so that the blank nanorings were formed without the encapsulation of fluorescent DEAC dyes in the silica matrix. Replacing the TMR dye conjugate with Cy5 dye conjugate for functionalization, inner/outer surface dye functionalization procedures described above were followed. The concentration of Cy5 dye for both inner and outer surface functionalizations was  $18~\mu\mathrm{M}$ .

Gel Permeation Chromatography (GPC). Following the dialysis step, the solutions were concentrated using spin filters (Vivaspin 20 MWCO 30k) in centrifugation (Eppendorf 5810R) at 4300 rpm for 45 min. The upconcentrated sample (400  $\mu$ L) was injected into a GPC column packed with a Superdex 200 prep grade resin using a 0.9 wt % sodium chloride saline as a buffer solution. Bio-Rad BioLogic LP system was used to operate the GPC column at a 2 mL/min flow rate, and Bio-Rad BioFrac was used to collect the GPC fractions of the samples at 14 s/fraction times absorbing at 275 nm. C rings were separated from the aggregation products and unreacted reagents via GPC fractionation, and collected samples were run in GPC again to check sample purity via the single-peak particle distribution. These are the GPC control runs reported in the main text to demonstrate sample purity.

High-Performance Liquid Chromatography (HPLC). All HPLC runs were carried out on a Waters Alliance 2965 separation module equipped with a column heater and a Waters 2996 photodiode array detector. The hardware was controlled by a computer running Empower 3 Feature Release 3. Deionized water was generated from a Millipore IQ7000 water system (18.2 MΩ resistivity), and acetonitrile was obtained from BDH (UHPLC grade). The columns used were 150 mm Waters Xbridge BEH C4 protein separation columns with a 300 Å pore size and a 3.5 μm particle size and 50 mm Waters Xbridge BEH C18 protein separation columns with a 300 Å pore size and a 3.5 μm particle size. All injections were 10 μL of 15 μM nanorings. Concentrations for injected samples were determined by FCS. For additional information, please see the Supporting Information.

**Transmission Electron Microscopy (TEM).** TEM samples were prepared by dropping  $\sim 8~\mu L$  of the sample solution diluted in ethanol onto a carbon-film-coated copper TEM grid and letting the sample air-dry on the grid on a filter paper. Dry-state TEM images were taken using an FEI Tecnai T12 Spirit microscope operated at 120 kV. Cryogenic electron microscopy (cryo-EM) was performed on a ring sample, as described in the literature.

Fluorescence Correlation Spectroscopy (FCS) of Fluorescent C Rings. Fluorescence correlation spectroscopy (FCS) measurements were performed on C rings encapsulating DEAC dye, using a home-built FCS setup with a HeNe 445 nm excitation source. FCS samples were prepared by diluting samples in water on a glass-bottom microwell dish. Photons were collected by an avalanche photodiode detector (SPCM 14, Perkin-Elmer). The photocurrent from the detector was digitally autocorrelated with a correlator card (Correlator.com). Before each set of measurements, the focal/observation volume was calibrated with 6CR110 as the standard dye such that the ratio of the radial to the axial radii of the focal volume is

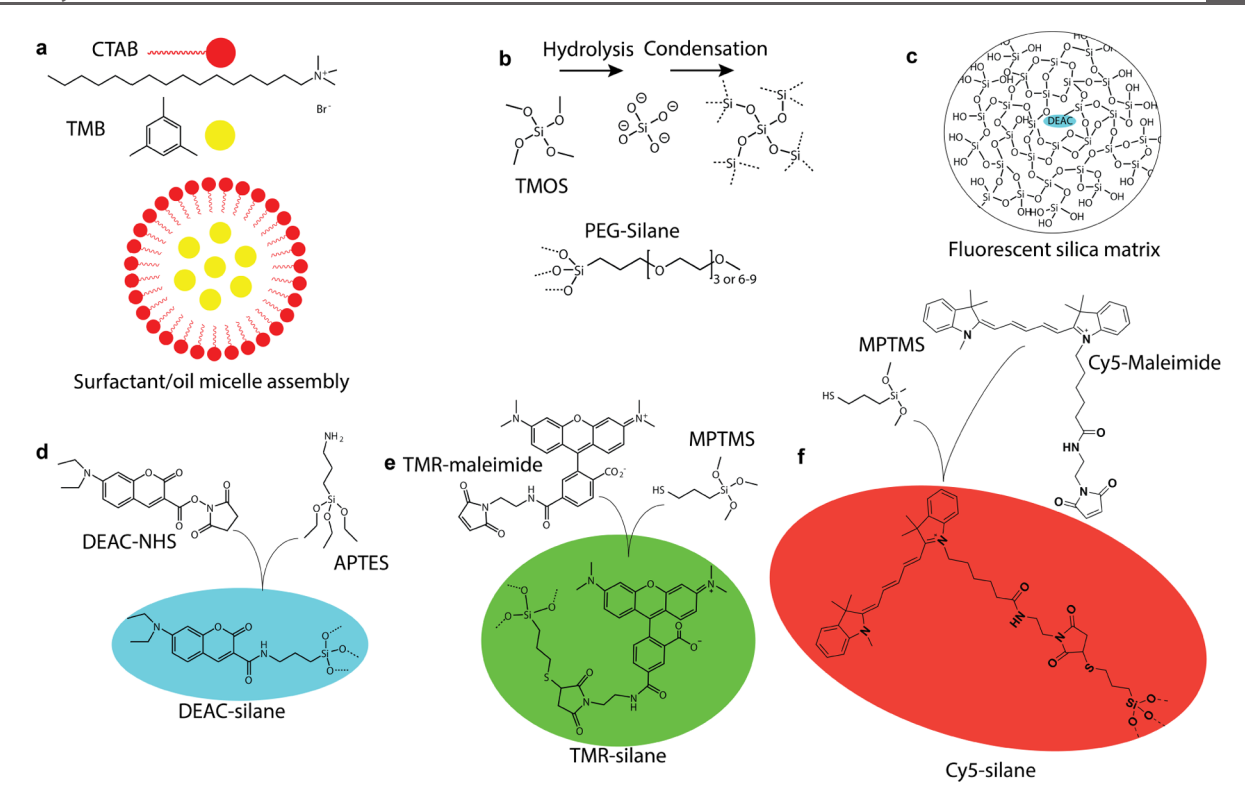


Figure 2. Molecular structure of compounds and silica networks, as well as dye-silane conjugation chemistry. (a) Chemical structures of surfactant (CTAB) and oil-pore expander (trimethyl benzene, TMB). (b) Hydrolysis and condensation steps of silica precursor (TMOS), and chemical structure of PEG-silane molecule. (c) Molecular rendering of DEAC dye encapsulating silica matrix. (d–f) Conjugation of the succinimidyl ester derivative of DEAC dye with aminopropyl-silane (d), as well as maleimido derivatives of TMR (e) and Cy5 dye (f) with mercaptopropyl-silane.

between 0.1 and 0.2. FCS autocorrelation curves were analyzed to obtain the hydrodynamic size, brightness per particle, and the concentration of the samples, as described in previous publications.<sup>32,33</sup> For additional information, please see the Supporting Information

**Steady-State Absorption Spectroscopy.** Varian Cary 5000 spectrophotometer was used to measure the absorption spectra of the samples in parallel to FCS measurements to calculate the number of dyes per particle as described in eq 3 below. To acquire the absorption spectra, first, a baseline subtraction against 3 mL of fresh deionized water in a quartz cuvette was performed. After the blank was measured, the sample was added directly to the cuvette and an absorption spectrum was acquired. The absorbance maxima of each sample were kept within the linear region of the Beer–Lambert law for concentration determinations and further calculations, as detailed in the Supporting Information.

## ■ RESULTS AND DISCUSSION

Orthogonal Pathways to Inner and Outer C Ring Surface Functionalizations. In recent reports, we have provided the full description of the synthesis approach to, and possible formation mechanism supported by in-depth structural characterization of, surfactant micelle-mediated formation of ultrasmall fluorescent silica nanorings (C rings). Figure 1 shows representative cryo- and transmission electron microscopy (cryo-EM/TEM) images of planar and edge-on views of a silica nanoring formed around a TMB-swollen CTAB micelle, originally used to unambiguously establish the ring geometry. Since the inner surface of C rings in the surfactant-mediated synthesis is originally shielded/covered by the surfactant micelle as illustrated in Figure 1, this micelle-directed formation mechanism should enable orthogonal functionalization of inner and outer C ring surfaces. As discussed in great

detail in our original paper first disclosing this ultrasmall ring structure, this effect is enhanced by the partial wrapping of the TMB-swollen micelle around the ring, driven by an electrostatic attraction between the positively charged micelle surface (from quaternary ammonia surfactant head groups) and the negatively charged silica surface (from deprotonated Si-OH groups). After the C ring synthesis as described in the Materials and Methods section, the inner surface is still covered by the micelle, while the outer bare silica surface is available for coating with a poly(ethylene glycol) layer (PEGylation step) and/or functionalization with other moieties as described in detail in earlier studies on conventional spherically shaped fluorescent core-shell SNPs with sizes below 10 nm referred to as Cornell dots or simply C dots.  $^{31,35}$  Once the outer silica surface is covered with these moieties, removal/etching of the surfactant micelles via, e.g., dialysis in acidic solutions (see Materials and Methods section) exposes the bare inner silica surface, which can subsequently be functionalized in an orthogonal fashion with other moieties of interest. Possible steps of such orthogonal functionalization schemes are schematically depicted in Figure 1, while the molecular structures of all chemical compounds used in the reactions described in this study are shown in Figure 2. To render the original C rings fluorescent for simple optical detection, we chose to work with the succinimidyl ester of 7diethylamino-coumarin-3-carboxylic acid (DEAC dye), which has an absorption maximum of around 440 nm, i.e., in the blue. This dye molecule can conveniently be reacted with APTES to provide a dye-silane conjugate (Figure 2d), which as a result of its neutral charge state and small size (MW ~ 350 g/mol), in turn, should get covalently encapsulated reasonably well into

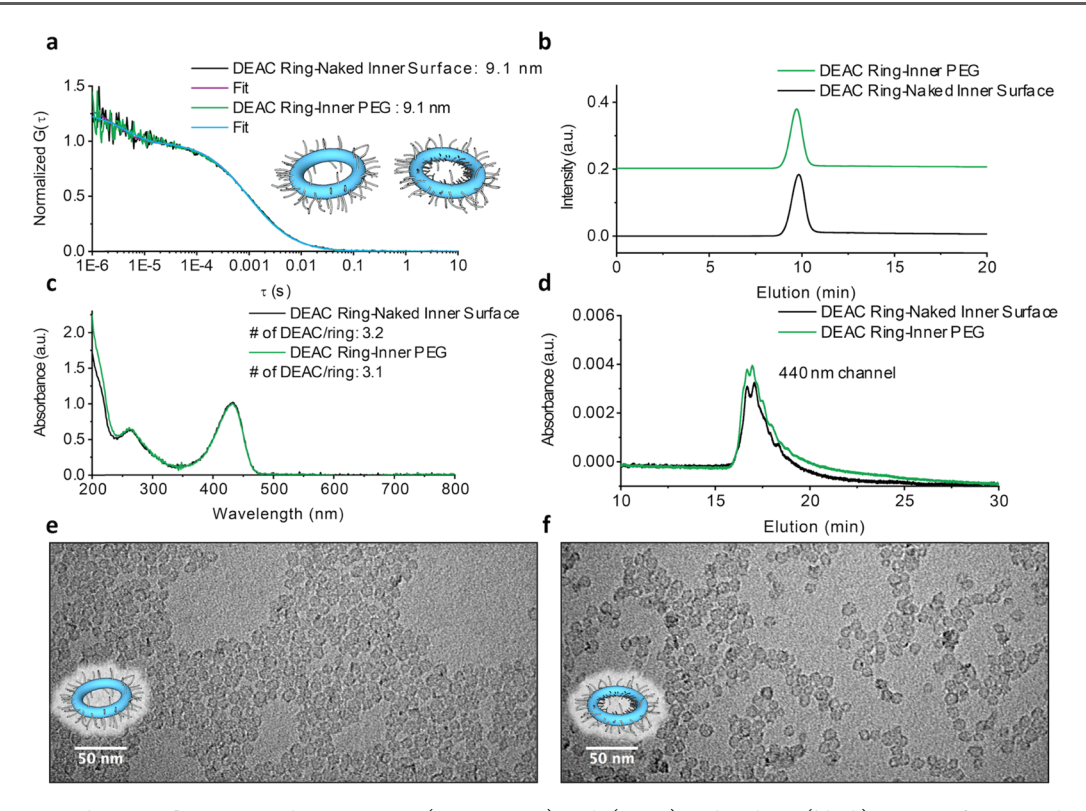


Figure 3. Comparison between fluorescent silica nanorings (DEAC rings) with (green) and without (black) inner surface PEGylation (with three EO-containing PEGs). (a) FCS autocorrelation curves suggesting 9.1 nm hydrodynamic sizes for both samples. (b) Analytical-scale GPC chromatograms of both samples. (c) Absorption spectra for the naked and inner-surface-PEGylated DEAC rings, suggesting (together with FCS results) 3.2 and 3.1 DEAC dyes per silica nanoring, respectively. (d) HPLC chromatograms at 440 nm readout channel (DEAC dye absorption). (e, f) TEM images of DEAC rings with naked (e) and PEGylated (f) inner surfaces.

the matrix of the silica rings.<sup>27</sup> DEAC-dye-containing rings are therefore rendered in blue in all figure schematics of this study.

In the first set of experiments to examine orthogonal functionalization pathways, the inner surface of silica nanorings, outer-surface-functionalized with a PEG-silane with 6-9 EO units, was either left naked or PEGylated using a 3 EO-chain length PEG-silane (Figure 2b). The same ring synthesis batch was used for the preparation of these two samples to minimize the effects of batch-to-batch synthesis variations. To that end, a mother batch was synthesized by taking the as-prepared C rings and PEGylating their outer silica surface. An aliquot of this batch was simply submitted to surfactant micelle removal/etching providing C rings with a bare inner surface, while a second aliquot underwent inner surface PEGylation after micelle etching. After final purification steps (see Materials and Methods section), to establish a baseline study, these two C ring samples underwent in-depth characterization via a combination of techniques (Figure 3) including FCS, GPC, absorption spectroscopy, HPLC, and TEM. FCS results (Figure 3a) suggested identical hydrodynamic sizes of 9.1 nm for both samples, corroborated by single-peak distributions and equal elution times in GPC (Figure 3b). A slightly higher absorption in the UV region of absorption spectra normalized to the 440 nm DEAC dye absorption maximum (Figure 3c) and characteristic for the presence of PEG, 21 was consistent with the successful inner surface PEGylation of the C rings (but may also indicate the insertion of additional smaller PEG moieties between existing PEG chains on the outer surface). Results of HPLC runs showed that both C rings elute at the same time and with similar peak shapes (Figure 3d), suggesting that in this

particular case of simple PEG coating of the inner surface versus bare silica, HPLC is not very sensitive to the details of the inner surface chemical properties. The shape and fine structure of the HPLC chromatograms with multiple peaks on a curve that first rises sharply and then tapers off at longer times are very similar to those observed for conventional PEGylated fluorescent C dots, suggesting incomplete encapsulation of one or more DEAC dyes leading to hydrophobic patches that prolong the corresponding elution times relative to a fully PEGylated surface.<sup>27</sup> Since the focus of the present study was a comparison of C rings with different inner and outer surface functionalities, we did not try to resolve these dye encapsulation details any further but rather used HPLC as a qualitative tool to compare different functionalized C rings. Finally, as expected, TEM images of the two C ring batches showed no discernible differences in particle morphology (compare Figure 3e,f).

Inner and Outer C Ring Surface Functionalizations with TMR Dye As Revealed by HPLC. Next, we functionalized either the inner or the outer surface of aliquots of the mother batch with zwitterionic (i.e., zero net charge) tetramethylrhodamine (TMR) dye, which has an absorption maximum of around 550 nm, well separated from that of the DEAC dye around 440 nm encapsulated into the silica ring matrix (vide supra). To that end, TMR-silane was first generated from the reaction of the maleimido derivative of TMR with mercaptopropyl-trimethoxysilane (MPTMS, Figure 2e). This dye derivative was then added to an aliquot of the mother batch either shortly before the addition of the PEG layer on the outer surface in the presence of the CTAB micelles covering the inner surface or after this PEGylation

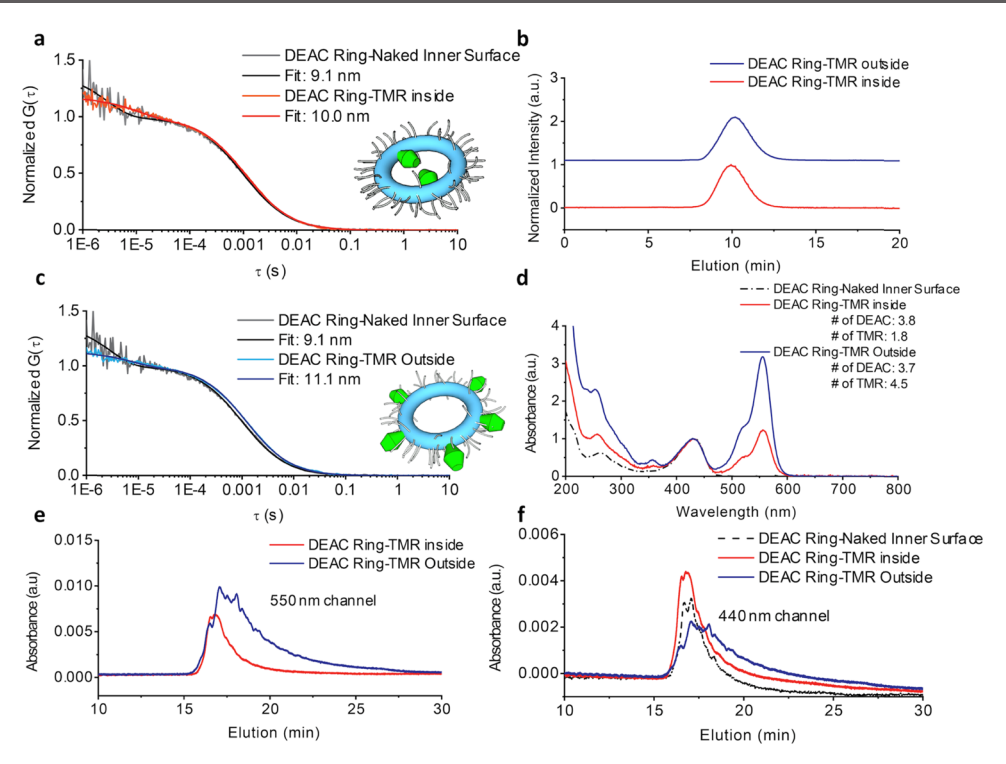


Figure 4. Comparison between DEAC rings with TMR functionalization inside (red) and outside (blue). (a, c) FCS autocorrelation curves suggesting hydrodynamic sizes of inside (a) and outside (c) TMR-functionalized DEAC rings of 10.0 and 11.1 nm, respectively, both larger than the reference DEAC rings with no extra functionality (9.1 nm, black). (b) GPC chromatograms of these two TMR-functionalized ring samples. (d) Absorption spectra of inside and outside TMR-functionalized DEAC rings compared to those of reference DEAC rings and normalized to DEAC absorption maximum at ~440 nm. Combination of absorption and FCS results confirms the same DEAC dye numbers for these two ring samples (3.8 and 3.7 dyes for inner- and outer-functionalized rings, respectively) but suggests different degrees of TMR functionalization with 1.8 and 4.5 TMR dyes for the inner- and outer-surface-functionalized rings, respectively. (e, f) HPLC chromatograms of inside and outside TMR-functionalized DEAC rings at a 550 nm readout channel (e, TMR dye absorption) and at a 440 nm readout channel (f, DEAC dye absorption). In (f), results are plotted against the reference DEAC rings with no TMR functionality (black curve).

step and micelle removal, thereby functionalizing the inner ring surface with TMR dye (see Materials and Methods section). In both cases, TMR-silane was added at the same concentration (40  $\mu$ M). Comparison of characterization results of these two C ring batches is shown in Figure 4. Figure 4a,c shows FCS correlation curves of inner (red) and outer (blue) surfacefunctionalized batches, respectively (i.e., carrying TMR dye on either the inner or outer surface while both encapsulating DEAC dye in the silica ring matrix), plotted against those of unfunctionalized C rings (DEAC dye carrying rings only, see Figure 3a). FCS data analysis suggested that the hydrodynamic particle size for the inner-surface-functionalized C rings increased from 9.1 to 10 nm, while that for the outersurface-functionalized rings increased from 9.1 to 11.1 nm when compared to that for the reference nanoring without TMR. Both functionalized samples showed a single-peak distribution in GPC (Figure 4b). The outside-functionalized C rings (blue) were slightly more size-dispersed, which correlates with the slightly larger-size increase observed in FCS. When comparing absorption spectra of the two TMR-functionalized ring batches normalized to the 440 nm absorption of the DEAC dye (Figure 4d), even though TMR-silane was added at the same concentration for both samples, it is apparent from the higher TMR absorption observed around 550 nm that there are substantially more TMR dyes on the outer (blue) than on the inner (red) surface. Combining information from FCS on particle concentration with these absorption results (see Materials and Methods), the number of TMR dyes per C

ring was determined to be 4.5 and 1.8 for outer and inner surface functionalizations, respectively, correlating well with the larger size for the former as detected by FCS. This higher dye number could be explained by the larger surface area available on the outside of the C rings, which translates into the availability of more surface silanol groups for TMR dyesilane attachment, as well as the higher accessibility of the outer versus the inner ring surface, which suggests steric hindrance of TMR functionalization of the inner surface once the first TMR dye is in place.

In addition to larger hydrodynamic C ring size from higher TMR dye numbers on the outer ring surface relative to the inner surface, HPLC chromatograms collected with a readout at 550 nm, the TMR dye absorption maximum, also showed substantial differences between these two batches (Figure 4e). Compared to the inner-surface-functionalized C rings (red), the outer-surface-functionalized rings (blue) had a wider distribution and tailing that indicates substantially increased nanoring hydrophobicity. Furthermore, using the 440 nm readout channel matching the DEAC dye absorption, HPLC results (Figure 4f) highlight that the inner-surface-functionalized nanorings (red curve) eluted at more similar times and exhibited a more similar elution profile to C rings with no inside or outside surface functionality (black curve) as compared to the outside-functionalized rings (blue). These results establish that in contrast to outer surface conjugations, functionalizing the inner ring surface with hydrophobic moieties, here TMR dyes, effectively "hides" these molecules

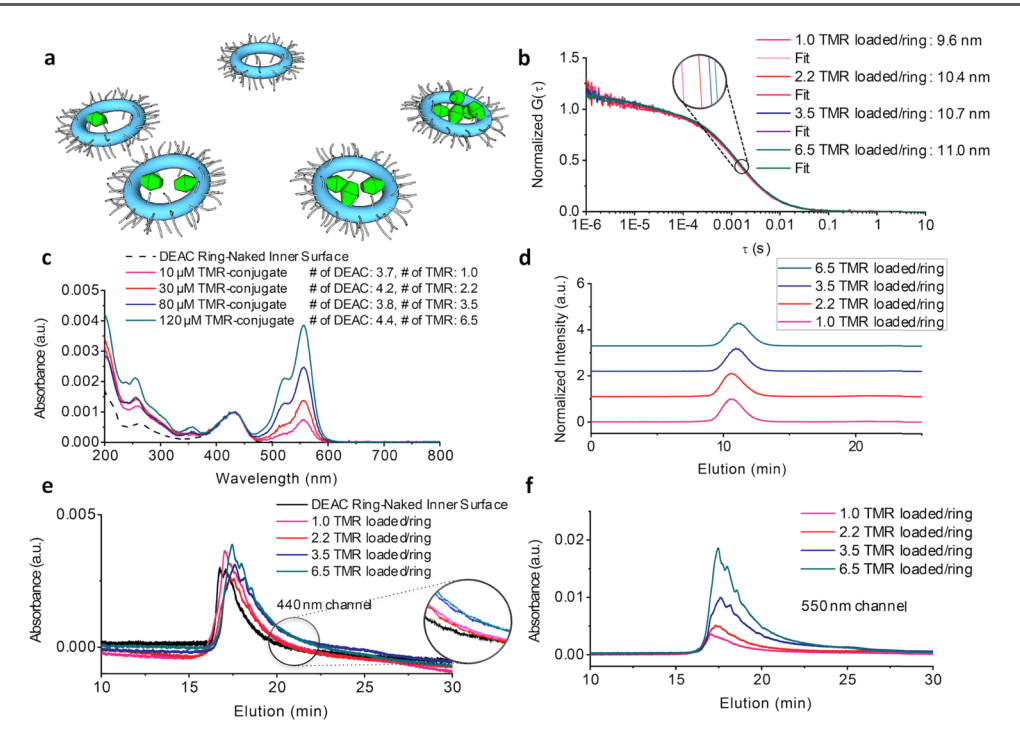


Figure 5. Comparison of DEAC rings with increasing inner surface functionalization with TMR dye. (a) Illustration of TMR loading to the inside surfaces of DEAC rings, where, as a function of TMR concentration in the synthesis, TMR dyes (shown in green) progressively get exposed to the ring outside as the number of TMR dyes per DEAC ring increases. (b) FCS autocorrelation curves of ring samples obtained from TMR dye concentrations in the synthesis of 10, 30, 80, and 120  $\mu$ M resulting in hydrodynamic sizes of 9.6, 10.4, 10.7, and 11.0 nm, respectively. (c) Absorption spectra of the same four samples as in (b) normalized to the 440 nm DEAC dye absorption. Together with FCS results from (b), these data suggest 3.7, 4.2, 3.8, and 4.4 DEAC dyes encapsulated in the silica ring matrix and 1.0, 2.2, 3.5, and 6.5 TMR dyes on the (inner) silica ring surface for each of the four batches, respectively. (d) GPC chromatograms of these four TMR-functionalized ring samples. (e, f) HPLC chromatograms of the same four TMR-functionalized DEAC ring batches as in (b)–(d) measured at the 440 nm readout channel (e, DEAC dye absorption) and the 550 nm readout channel (f, TMR dye absorption). In (e), HPLC data of the four ring batches are compared to the results of the parent (non-TMR-functionalized, naked) rings (black curve).

in the pore of these ultrasmall nanorings, thereby shielding them from interactions with their environment. Taken together, the preceding results unambiguously demonstrate that we are able to selectively functionalize the inner versus the outer surface of ultrasmall silica nanorings and that HPLC is a powerful experimental tool to differentiate between these two functionalization sites. In addition to the relatively rapid (short elution time) screening HPLC method (referred to as method 2) employed here, we also applied our previously developed more quantitative HPLC method (referred to as method 1 with longer elution times)<sup>27</sup> to both ring samples described in Figures 3 and 4. These studies summarized in Supporting Information Figure S1 demonstrate that for DEAC and TMRfunctionalized rings, HPLC results were robust against changes in both the HPLC parameters and columns. This is encouraging as it suggests that a variety of HPLC separation methods may be successful in differentiating between these types of chemical differences and that it may be possible to extend these chromatographic methods to other ultrasmall nanomaterial compositions and morphologies.

Assessing "Effective" Inner Ring Surface Loading Capacity by HPLC. The ability to distinguish between inner and outer surface functionalizations via HPLC allowed us to determine an effective cargo loading capacity of the inner surface of C rings, i.e., the loading capacity for which a particular hydrophobic cargo can effectively be "hidden" in the pore. The loading capacity is a crucial parameter, e.g., in the context of the delivery of drugs and other pharmaceutically

relevant molecules to sites of disease. Once the effective loading capacity of the inside surface of the nanorings is reached, further functionalization may still occur but only on the outer surface of the nanorings exposing the cargo to interactions with the environment. To assess this quantity, the inner surface of C rings encapsulating DEAC dye in their silica matrix was functionalized employing increasing concentrations of TMR-silane (10, 30, 80, and 120  $\mu$ M) using the same approaches as described before (see Materials and Methods). With a silica wall thickness of only around 2 nm, a nanoring pore size of around 6 nm, and a TMR-silane conjugate size of somewhere between 2 and 3 nm (Supporting Information Figure S2), i.e., roughly equal to pore radius, as illustrated in Figure 5a, we expected to see TMR dye being pushed toward the outside of the nanorings as the number of TMR dyes per nanoring increases beyond 2 (Figure 5a). This is consistent with what was experimentally observed via HPLC. Analysis of FCS measurements (Figure 5b) combined with that of absorption spectra (Figure 5c) normalized to the 440 nm DEAC dye peak of the four C ring samples obtained from increasing TMR-silane precursor in the synthesis suggested increasing hydrodynamic sizes of 9.6, 10.4, 10.7, and 11.0 nm, as well as 1.0, 2.2, 3.5, and 6.5 TMR dyes per nanoring, respectively. The associated GPC distributions got progressively more disperse as the number of TMR-silane per nanoring increased (Figure 5d). In the corresponding HPLC chromatograms taken at 440 nm (DEAC dye) and 550 nm (TMR dye) readouts, see Figure 5e,f, respectively, relative to

the unfunctionalized rings (black curve in Figure 5e), we saw increasing shifts and tailing toward longer elution times/more hydrophobic behavior, in particular, for C rings with more than two dyes per particle. As schematically illustrated in Figure 5a, this suggests a shift from well-hidden TMR dyes in the pore to more and more TMR dyes exposed to the outside, leading to an increasingly hydrophobic nanoring behavior. Once the ring pore is significantly overloaded, the cargo is exposed to the outside so much that these inner-functionalized rings become more hydrophobic than outside-functionalized rings. This is demonstrated in Figure 6a, where HPLC traces from a ring

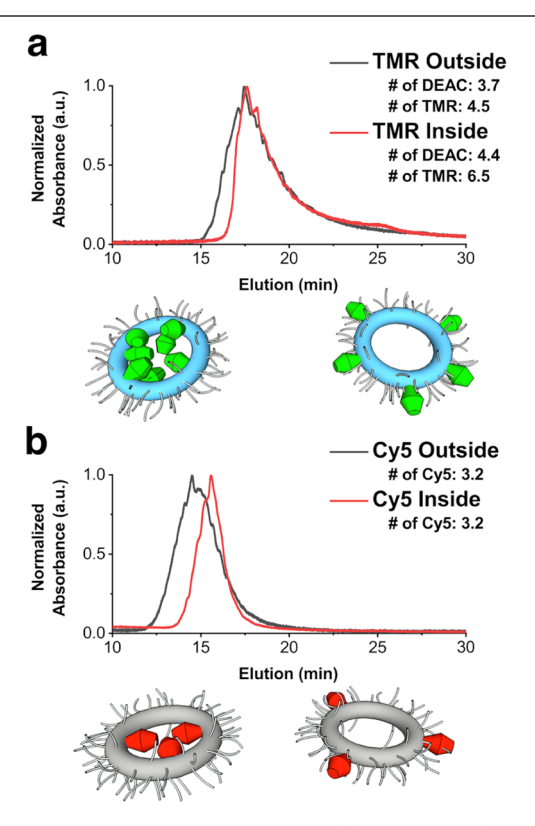


**Figure 6.** HPLC chromatograms at (a) 550 nm (TMR dye absorption) and (b) 647 nm (Cy5 dye absorption) readout channels for inside/outside TMR dye-loaded DEAC rings and inside/outside Cy5 dye-loaded blank silica rings, respectively.

with 6 to 7 TMR molecules on the inside begin eluting at later retention times as compared to a ring with 4 to 5 TMR molecules on the outside (see schematic), suggesting a more hydrophobic character for the inner-functionalized ring. This result demonstrates the critical importance of elucidating the effective loading capacity of the ring pore, as overloading the ring pore renders the vehicle more hydrophobic than the functionalization of the outside surface. It is important to note that the rings overloaded on the inside are likely more hydrophobic than the outside-functionalized rings because hydrophobic ligands on the outside may benefit from partial shielding by the hydrophilic PEG layer. The inside surface was left unPEGylated so that hydrophilic versus hydrophobic behavior depended primarily on localization and "hiding" of the hydrophobic cargo within the pore, which we wanted to elucidate.

HPLC-Derived Effective Inner Ring Loading Capacity as a Function of Cargo Size and Charge. One would expect that the effective inner ring loading capacity is sensitive

to the size of the hydrophobic cargo relative to the pore size. In other words, the larger the hydrophobic cargo, the more difficult it is to hide it on the inside of the single pore of the ring. To test this hypothesis, we functionalized inner and outer surfaces of C rings with a Cy5 derivative of a net positive charge (see Materials and Methods and Figure 2f), a fluorescent dye belonging to the cyanine dye family that is larger than TMR (see Supporting Information Figure S2). Both inner- and outer-surface-functionalized samples carried the same number of Cy5 dyes (n = 3.2 from FCS/UV-vis, see Supporting Information Figure S3), thus removing the need for DEAC as a reference dye (i.e., no DEAC dye was used in the silica ring matrix; see the synthesis of blank C rings in Experimental Section). As a first indication, fully characterized rings with an equal number of Cy5 dyes on either the ring inside or ring outside showed an increase in the left absorption shoulder of Cy5 around 600 nm for the inner-surfacefunctionalized material (red data set). Since this shoulder is sensitive to dye aggregation,<sup>36</sup> this result is consistent with dye crowding on the inside (Supporting Information Figure S3c). When applying our qualitative HPLC screening method (method 2 in Figure S1) to these inside and outside surfacefunctionalized rings, chromatograms for rings with three Cy5 dyes on the inside started to elute at later times than those with Cy5 on the outside, suggesting more hydrophobic behavior (Figure 6b), consistent with dye-overloading effects of the inner ring surface already becoming predominant for dye numbers as low as 3. Moreover, comparing this effect for Cy5 with the results for TMR (Figure 6a) reveals larger-onset shifts between the two chromatograms for Cy5 consistent with the expected size effect. It is interesting to note that overall the position of both Cy5 chromatograms is shifted to smaller retention times relative to the two TMR traces. We believe that this overall shift is due to the absence of DEAC in the Cy5modified rings, supported by the fact that the HPLC peak structure and tailing to larger retention times observed in Figure 3D are all due to DEAC only partially incorporated into the silica matrix of the C rings, thereby rendering these rings more hydrophobic than their undyed counterparts (vide supra).

We finally tried to functionalize the blank C rings using a Cy5 dye derivative with a net negative charge. While this worked for the outer surface, it did not for the inner surface of the nanorings (data not shown). This is most likely due to repulsive electrostatic interactions between the negatively charged Cy5 dye and the negatively charged naked inner surface of C rings (from deprotonated silanol surface groups), an effect that is screened by the PEG chains on the outer surface. As shown above, neither zwitterionic TMR dye that is charge neutral nor positively charged Cy5 (Supporting Information Figure S2) suffered from this problem, further supporting this interpretation.

## CONCLUSIONS

In this study, we synthesized a class of nonspherical ultrasmall fluorescent silica nanoparticles in the form of rings (C rings) that were surface-functionalized on chemically and spatially distinct inner and outer surfaces, respectively. We demonstrated that reversed-phase HPLC is a sensitive tool able to distinguish between samples orthogonally functionalized on these surfaces with model dye-silane conjugates of different hydrophobicity, size, and charge. Results suggest that despite the small silica hydrodynamic ring size of 10 nm and below it is

possible to "hide" hydrophobic moieties on the inside of the rings, but that to accomplish this effectively, their number must be carefully engineered. We expect the class of ultrasmall nanorings described here to be of relevance for both diagnostic and drug delivery applications in nanomedicine. Furthermore, we anticipate that the chromatographic methods developed to characterize multiple spatially and chemically distinct surface chemistries on these nanoparticles will be applicable to a range of differently shaped porous nanoparticles within the ultrasmall-size regime.

## ASSOCIATED CONTENT

## **S** Supporting Information

The Supporting Information is available free of charge on the ACS Publications website at DOI: 10.1021/acs.chemmater.9b01236.

Comparison of results from HPLC method 1 and method 2 (Figure S1); molecular structures and dimensions of "stretched" TMR-silane and Cy5-silane dye conjugates (Figure S2); and characterization of plain rings with inner and outer surfaces functionalized with Cy5 dye (Figure S3) (PDF)

#### AUTHOR INFORMATION

#### **Corresponding Author**

\*E-mail: ubw1@cornell.edu. Fax: 607-255-2365.

#### ORCID ®

Melik Z. Turker: 0000-0001-7801-4275 Thomas C. Gardinier: 0000-0002-9442-3770 Joshua A. Hinckley: 0000-0002-0575-5045

Kai Ma: 0000-0003-4415-6894

Ferdinand F. E. Kohle: 0000-0002-7351-5940 Ulrich B. Wiesner: 0000-0001-6934-3755

### **Author Contributions**

\*M.Z.T. and T.C.G. contributed equally to this work.

## **Author Contributions**

M.Z.T., T.C.G., K.M., and U.B.W. designed experiments. M.Z.T., J.A.H., and F.F.E.K. performed FCS measurements. M.Z.T., F.W., and C.B.C. synthesized fluorescent nanorings. T.C.G. developed methods and performed HPLC. M.Z.T. performed TEM.

#### **Notes**

The authors declare the following competing financial interest(s): U.W. and K.M have a financial interest in Elucida Oncology, Inc. T.G., M.Z.T., and U.W. have filed for a patent based on these findings. Other authors declare no competing interests.

## ACKNOWLEDGMENTS

This work was funded by the National Cancer Institute of the National Institutes of Health (NIH) under Award Number U54CA199081. HPLC and GPC experiments were supported by MC<sup>2</sup>TCN Center for Cancer Nanotechnology Excellence, which is also supported by NIH under Award Number U54CA199081. The authors thank John Grazul and the Cornell Center for Materials Research (CCMR) for the use of the electron microscopy facilities, which are supported by the National Science Foundation MRSEC program under Award Number DMR-1719875. M.Z.T. thanks the Ministry of National Education of the Republic of Turkey for his student scholarship support. C.B.C. thanks the Fullbright Program for

her postdoctoral visitor scholarship support. The authors gratefully thank K. A. Spoth and L. F. Kourkoutis for cryo-EM help.

#### REFERENCES

- (1) Jadzinsky, P. D.; Calero, G.; Ackerson, C. J.; Bushnell, D. A.; Kornberg, R. D. Structure of a Thiol Monolayer–Protected Gold Nanoparticle at 1.1 Å Resolution. *Science* **2007**, *318*, 430–433.
- (2) Turner, M.; Golovko, V. B.; Vaughan, O. P.; Abdulkin, P.; Berenguer-Murcia, A.; Tikhov, M. S.; Johnson, B. F.; Lambert, R. M. Selective Oxidation with Dioxygen by Gold Nanoparticle Catalysts Derived from 55-Atom Clusters. *Nature* **2008**, *454*, 981–983.
- (3) Phillips, E.; Penate-Medina, O.; Zanzonico, P. B.; Carvajal, R. D.; Mohan, P.; Ye, Y.; Humm, J.; Gonen, M.; Kalaigian, H.; Schoder, H.; Strauss, H. W.; Larson, S. M.; Wiesner, U.; Bradbury, M. S. Clinical Translation of an Ultrasmall Inorganic Optical-PET Imaging Nanoparticle Probe. *Sci. Transl. Med.* **2014**, *6*, No. 260ra149.
- (4) Park, J. H.; von Maltzahn, G.; Zhang, L.; Schwartz, M. P.; Ruoslahti, E.; Bhatia, S. N.; Sailor, M. J. Magnetic Iron Oxide Nanoworms for Tumor Targeting and Imaging. *Adv. Mater.* **2008**, *20*, 1630–1635.
- (5) Jana, N. R.; Gearheart, L.; Murphy, C. J. Wet Chemical Synthesis of High Aspect Ratio Cylindrical Gold Nanorods. *J. Phys. Chem. B* **2001**, *105*, 4065–4067.
- (6) Ma, K.; Gong, Y.; Aubert, T.; Turker, M. Z.; Kao, T.; Doerschuk, P. C.; Wiesner, U. Self-Assembly of Highly Symmetrical, Ultrasmall Inorganic Cages Directed by Surfactant Micelles. *Nature* **2018**, 558, 577–580.
- (7) Tessonnier, J. P.; Ersen, O.; Weinberg, G.; Pham-Huu, C.; Su, D. S.; Schlogl, R. Selective Deposition of Metal Nanoparticles Inside or Outside Multiwalled Carbon Nanotubes. *ACS Nano* **2009**, *3*, 2081–2089.
- (8) Zhao, Z.; Jacovetty, E. L.; Liu, Y.; Yan, H. Encapsulation of Gold Nanoparticles in a DNA Origami Cage. *Angew. Chem., Int. Ed.* **2011**, *50*, 2041–2044.
- (9) Ma, K.; Spoth, K. A.; Cong, Y.; Zhang, D.; Aubert, T.; Turker, M. Z.; Kourkoutis, L. F.; Mendes, E.; Wiesner, U. Early Formation Pathways of Surfactant Micelle Directed Ultrasmall Silica Ring and Cage Structures. *J. Am. Chem. Soc.* **2018**, *140*, 17343–17348.
- (10) Tang, F.; Li, L.; Chen, D. Mesoporous Silica Nanoparticles: Synthesis, Biocompatibility and Drug Delivery. *Adv. Mater.* **2012**, *24*, 1504–1534.
- (11) Lee, J. E.; Lee, N.; Kim, T.; Kim, J.; Hyeon, T. Multifunctional Mesoporous Silica Nanocomposite Nanoparticles for Theranostic Applications. *Acc. Chem. Res.* **2011**, *44*, 893–902.
- (12) Chen, A. M.; Zhang, M.; Wei, D.; Stueber, D.; Taratula, O.; Minko, T.; He, H. Co-Delivery of Doxorubicin and Bcl-2 siRNA by Mesoporous Silica Nanoparticles Enhances the Efficacy of Chemotherapy in Multidrug-Resistant Cancer Cells. *Small* **2009**, *5*, 2673–2677.
- (13) Choi, H. S.; Liu, W.; Misra, P.; Tanaka, E.; Zimmer, J. P.; Itty Ipe, B.; Bawendi, M. G.; Frangioni, J. V. Renal Clearance of Quantum Dots. *Nat. Biotechnol.* **2007**, *25*, 1165–1170.
- (14) Burns, A. A.; Vider, J.; Ow, H.; Herz, E.; Penate-Medina, O.; Baumgart, M.; Larson, S. M.; Wiesner, U.; Bradbury, M. Fluorescent Silica Nanoparticles with Efficient Urinary Excretion for Nanomedicine. *Nano Lett.* **2009**, *9*, 442–448.
- (15) Ma, K.; Sai, H.; Wiesner, U. Ultrasmall Sub-10 nm Near-Infrared Fluorescent Mesoporous Silica Nanoparticles. *J. Am. Chem. Soc.* **2012**, *134*, 13180–13183.
- (16) Ma, K.; Werner-Zwanziger, U.; Zwanziger, J.; Wiesner, U. Controlling Growth of Ultrasmall Sub-10 nm Fluorescent Mesoporous Silica Nanoparticles. *Chem. Mater.* **2013**, *25*, *677*–*691*.
- (17) Chen, F.; Ma, K.; Madajewski, B.; Zhuang, L.; Zhang, L.; Rickert, K.; Marelli, M.; Yoo, B.; Turker, M. Z.; Overholtzer, M.; Quinn, T. P.; Gonen, M.; Zanzonico, P.; Tuesca, A.; Bowen, M. A.; Norton, L.; Subramony, J. A.; Wiesner, U.; Bradbury, M. S. Ultrasmall Targeted Nanoparticles with Engineered Antibody Fragments for

Imaging Detection of HER2-Overexpressing Breast Cancer. *Nat. Commun.* **2018**, 9, No. 4141.

- (18) Chen, F.; Ma, K.; Zhang, L.; Madajewski, B.; Zanzonico, P.; Sequeira, S.; Gonen, M.; Wiesner, U.; Bradbury, M. S. Target-or-Clear Zirconium-89 Labeled Silica Nanoparticles for Enhanced Cancer-Directed Uptake in Melanoma: A Comparison of Radiolabeling Strategies. *Chem. Mater.* **2017**, 29, 8269–8281.
- (19) Shin, J.; Anisur, R. M.; Ko, M. K.; Im, G. H.; Lee, J. H.; Lee, I. S. Hollow Manganese Oxide Nanoparticles as Multifunctional Agents for Magnetic Resonance Imaging and Drug Delivery. *Angew. Chem., Int. Ed.* **2009**, *48*, 321–324.
- (20) Santra, S.; Kaittanis, C.; Grimm, J.; Perez, J. M. Drug/Dye-Loaded, Multifunctional Iron Oxide Nanoparticles for Combined Targeted Cancer Therapy and Dual Optical/Magnetic Resonance Imaging. *Small* **2009**, *5*, 1862–1868.
- (21) Ma, K.; Wiesner, U. Modular and Orthogonal Post-PEGylation Surface Modifications by Insertion Enabling Penta-Functional Ultrasmall Organic-Silica Hybrid Nanoparticles. *Chem. Mater.* **2017**, *29*, 6840–6855.
- (22) Jones, M. R.; Macfarlane, R. J.; Lee, B.; Zhang, J.; Young, K. L.; Senesi, A. J.; Mirkin, C. A. DNA-Nanoparticle Superlattices Formed from Anisotropic Building Blocks. *Nat. Mater.* **2010**, *9*, 913–917.
- (23) Vivero-Escoto, J. L.; Slowing, I. I.; Trewyn, B. G.; Lin, V. S. Mesoporous Silica Nanoparticles for Intracellular Controlled Drug Delivery. *Small* **2010**, *6*, 1952–1967.
- (24) Cho, E. J.; Holback, H.; Liu, K. C.; Abouelmagd, S. A.; Park, J.; Yeo, Y. Nanoparticle Characterization: State of the Art, Challenges, and Emerging Technologies. *Mol. Pharmaceutics* **2013**, *10*, 2093–2110.
- (25) Mullen, D. G.; Desai, A. M.; Waddell, J. N.; Cheng, X. M.; Kelly, C. V.; McNerny, D. Q.; Majoros, I. J.; Baker, J. R., Jr.; Sander, L. M.; Orr, B. G.; Banaszak Holl, M. M. The Implications of Stochastic Synthesis for the Conjugation of Functional Groups to Nanoparticles. *Bioconjugate Chem.* **2008**, *19*, 1748–1752.
- (26) Mullen, D. G.; Fang, M.; Desai, A.; Baker, J. R.; Orr, B. G.; Banaszak Holl, M. M. A Quantitative Assessment of Nanoparticle-Ligand Distributions: Implications for Targeted Drug and Imaging Delivery in Dendrimer Conjugates. *ACS Nano* **2010**, *4*, 657–670.
- (27) Gardinier, T. C.; Kohle, F. F. E.; Peerless, J. S.; Ma, K.; Turker, M. Z.; Hinckley, J. A.; Yingling, Y. G.; Wiesner, U. High-Performance Chromatographic Characterization of Surface Chemical Heterogeneities of Fluorescent Organic-Inorganic Hybrid Core-Shell Silica Nanoparticles. ACS Nano 2019, 13, 1795—1804.
- (28) Masters, C. L.; Simm, G.; Weinman, N. A.; Multhaup, G.; McDonald, B. L.; Beyreuther, K. Amyloid Plaque Core Protein in Alzheimer Disease and Down Syndrome. *Proc. Natl. Acad. Sci. U.S.A.* 1985, 82, 4245–4249.
- (29) Lee, M. S.; Kerns, E. H. LC/MS Applications in Drug Development. *Mass Spectrom. Rev.* **1999**, *18*, 187–279.
- (30) Peng, J.; Elias, J. E.; Thoreen, C. C.; Licklider, L. J.; Gygi, S. P. Evaluation of Multidimensional Chromatography Coupled with Tandem Mass Spectrometry (LC/LC-MS/MS) for Large-Scale Protein Analysis: The Yeast Proteome. *J. Proteome Res.* **2003**, 2, 43–50.
- (31) Ma, K.; Zhang, D.; Cong, Y.; Wiesner, U. Elucidating the Mechanism of Silica Nanoparticle PEGylation Processes Using Fluorescence Correlation Spectroscopies. *Chem. Mater.* **2016**, 28, 1537–1545.
- (32) Larson, D. R.; Ow, H.; Vishwasrao, H. D.; Heikal, A. A.; Wiesner, U.; Webb, W. W. Silica Nanoparticle Architecture Determines Radiative Properties of Encapsulated Fluorophores. *Chem. Mater.* **2008**, *20*, 2677–2684.
- (33) Kohle, F. F. E.; Hinckley, J. A.; Li, S.; Dhawan, N.; Katt, W. P.; Erstling, J. A.; Werner-Zwanziger, U.; Zwanziger, J.; Cerione, R. A.; Wiesner, U. B. Amorphous Quantum Nanomaterials. *Adv. Mater.* **2019**, No. 1806993.
- (34) Turker, M. Z.; Ma, K.; Wiesner, U. B. Bimodal Morphology Transition Pathway in the Synthesis of Ultrasmall Fluorescent

Mesoporous Silica Nanoparticles. J. Phys. Chem. C 2019, 123, 9582–9589.

- (35) Ma, K.; Mendoza, C.; Hanson, M.; Werner-Zwanziger, U.; Zwanziger, J.; Wiesner, U. Control of Ultrasmall Sub-10 nm Ligand-Functionalized Fluorescent Core—Shell Silica Nanoparticle Growth in Water. *Chem. Mater.* **2015**, 27, 4119–4133.
- (36) Berlepsch, H. v.; Bottcher, C. H-Aggregates of an Indocyanine Cy5 Dye: Transition from Strong to Weak Molecular Coupling. *J. Phys. Chem. B* **2015**, *119*, 11900–11909.